

# LEVERAGING SCALE-INVARIANCE AND UNCERTAINTY WITH SELF-SUPERVISED DOMAIN ADAPTATION FOR SEMANTIC SEGMENTATION OF FOGGY SCENES

Javed Iqbal\*, Rehan Hafiz, Mohsen Ali

Information Technology University, Lahore, Pakistan - {javed.iqbal, rehan.hafiz, mohsen.ali}@itu.edu.pk

**KEY WORDS:** Foggy Scene Understanding, Semantic Segmentation, Self-supervised Learning, Domain Adaptation.

## ABSTRACT:

This paper presents FogAdapt, a novel approach for domain adaptation of semantic segmentation for dense foggy scenes. Although significant research has been directed to reduce the domain shift in semantic segmentation, adaptation to scenes with adverse weather conditions remains an open question. Large variations in the visibility of the scene due to weather conditions, such as fog, smog, and haze, exacerbate the domain shift, thus making unsupervised adaptation in such scenarios challenging. We propose a self-entropy and multi-scale information augmented self-supervised domain adaptation method (FogAdapt) to minimize the domain shift in foggy scenes segmentation. Supported by the empirical evidence that an increase in fog density results in high self-entropy for segmentation probabilities, we introduce a self-entropy based loss function to guide the adaptation method. Furthermore, inferences obtained at different image scales are combined and weighted by the uncertainty to generate scale-invariant pseudo-labels for the target domain. These scale-invariant pseudo-labels are robust to visibility and scale variations. We evaluate the proposed model on real clear-weather scenes to real foggy scenes adaptation and synthetic non-foggy images to real foggy scenes adaptation scenarios. Our experiments demonstrate that FogAdapt significantly outperforms the current state-of-the-art in semantic segmentation of foggy images. Specifically, by considering the standard settings compared to state-of-the-art (SOTA) methods, FogAdapt gains 3.8% on Foggy Zurich, 6.0% on Foggy Driving-dense, and 3.6% on Foggy Driving in mIoU when adapted from Cityscapes to Foggy Zurich.

## 1. INTRODUCTION

Semantic segmentation is one of the important components of autonomous systems, i.e., self-driving cars [Geiger et al., 2012]. Deep Learning approaches for semantic segmentation, relying on the large tagged datasets [Cordts et al., 2016, Ros et al., 2016], have resulted in substantially improved performance [Sakaridis et al., 2018a, Zhao et al., 2017, Chen et al., 2018a] in the last few years. However, similar to many other supervised learning problems [Khodabandeh et al., 2019, Marsde et al., 2018], semantic segmentation models exhibit large generalization errors [Zou et al., 2018, Vu et al., 2019a, Subhani and Ali, 2020]. This behavior is ascribed to the domain shift between the distribution of the test and training data domains [Zhang et al., 2017, Lian et al., 2019]. One of the challenging case of the domain adaptation could be attributed to weather conditions such as rain, fog, snowfall, lightning and strong wind [Chen et al., 2019, Sakaridis et al., 2018a, Vachmanus et al., 2020]. Fog specifically degrades the visibility and contrast significantly [Narasimhan and Nayar, 2003, Tan, 2008], deteriorating the performance of the computer vision applications, e.g., segmentation. Domain adaptation algorithms have been presented to overcome the domain shift (synthetic to real [Tsai et al., 2018, Zou et al., 2018, Iqbal and Ali, 2020a] or real to real [Chen et al., 2017] datasets) specific to the case of semantic segmentation. However, very little attention has been devoted to address domain shift caused by foggy weather conditions [Sakaridis et al., 2018b, Sakaridis et al., 2018a, Dai et al., 2019].

In this work, we present a novel self-supervised domain adaptation method, *FogAdapt*, for semantic segmentation of images captured in dense foggy weather. In foggy conditions, the image contrast and color quality drop significantly degrading the clarity and visibility of the scene. This occurs due to the presence of particles in the atmosphere which scatter and absorb light [Tan, 2008, Narasimhan and Nayar, 2003]. Since these particles might

be non-uniformly present in different parts of the scene, fog could eventually be of different densities at different locations. Similarly, depending upon the distance between the camera and the objects, fog affects the visibility of objects differently. Specifically, the visibility is decreased with increasing distance, e.g., the farthest objects are more difficult to recognize. An illustration is shown in Fig. 1, where keeping everything else constant, as the fog density is varied from clear to dense, the corresponding semantic segmentation deteriorates accordingly, with the farthest regions most affected. Combination of these variations results in a considerably large set of scenarios, making collection and labeling costly and laborious, especially for the semantic segmentation and robust supervised learning techniques. Hence, need for a robust unsupervised domain adaptation (UDA) method for such a challenging scenario of dense fog in the target images.

To counter the challenges posed by domain shift in dense foggy scenes, we present a novel self-supervised domain adaptation method (FogAdapt) for UDA of foggy scenes segmentation. Our domain (fog) specific empirical analysis led us to discover relationships between the effect of fog and road-scene segmentation. We exploit the relationship between **uncertainty, measured by self-entropy**, and the density of fog (Fig. 2) by defining a self-entropy minimization loss for the target images, when a source (clear weather images) trained semantic segmentation model is utilized for the target (foggy image) dataset. Similarly, we explore the image scale and fog relationship (Fig. 3) and generate pseudo-labels at pixel level by exploiting the consistency constraint over image scaling to counter the effect of fog. Below we discuss in detail the empirical analysis and the proposed solution specifically designed to counter the effects of fog with further details in Section 3.

*Self Entropy loss & Fog Density:* Images taken in fog exhibit degradation of color quality, low contrast, and other artifacts associated with low visibility. Overall this results in images with texture, edges, and color information deteriorated enough to make it difficult to differentiate between different objects and

\*Corresponding author

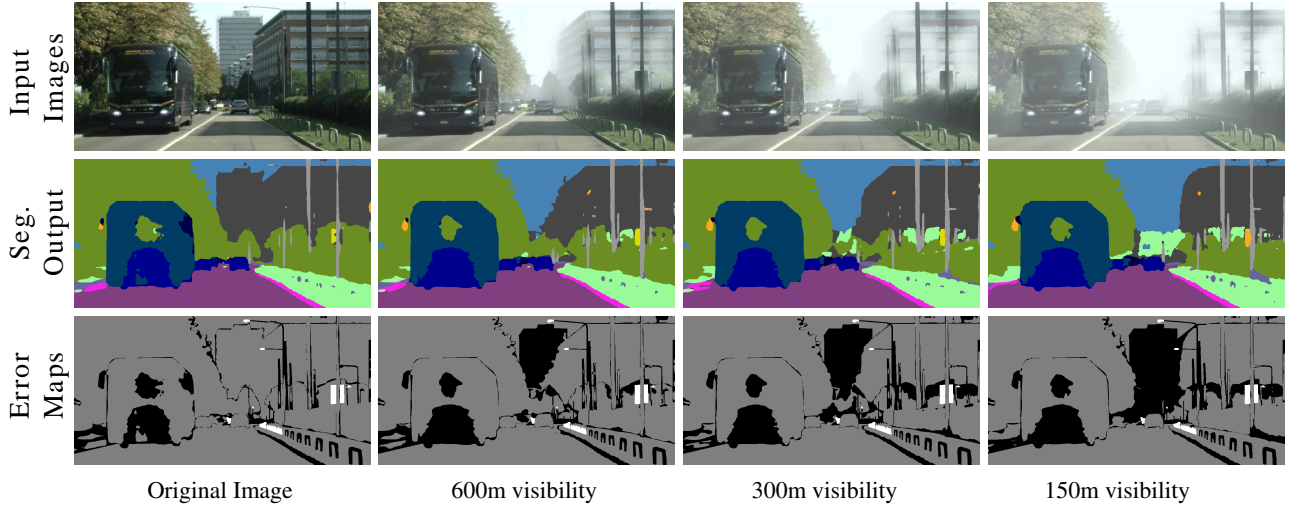


Figure 1: Image contrast and color quality degradation due to fog and resultant deterioration in the segmentation performance. Row-1: images with decreasing visibility. Row-2: corresponding segmentation outputs. Row-3: error maps, where the **grey** and **black** regions show correct and erroneous segmentation respectively, while the **white** regions are untagged. The segmentation performance deteriorates with increasing fog density. (The results are generated using a clear weather GTA to Cityscapes adapted model).

stuff classes. This loss of information results in a confusing semantic segmentation network (trained in normal weather), making it unable to differentiate between different category pixels, resulting in high self-entropy. This relationship between the self-entropy and the density of the fog has been presented in Fig. 2. To observe how the self-entropy changes with respect to the fog-density, we use Foggy-Cityscapes, a simulated fog added real imagery dataset [Sakaridis et al., 2018a], where the same images and their foggy versions at multiple visibility ranges are available. We manually choose and extract small patches ( $100 \times 150$  pixels) from the same locations of the normal images and their modified versions with simulated dense and moderate fog added to it. Self-entropy maps are computed for each patch after passing these images through semantic segmentation network, **trained on GTA non-foggy images**. Few of them are shown in Fig. 2. The three distributions obtained for all the extracted patches at respective fog levels (Fig. 2 (a)), visualized in Fig. 2 (b), indicate a strong relationship between fog density and self-entropy, i.e., the denser the fog, the higher the self-entropy. This lead us to our hypothesis that minimizing the self-entropy may force the network to learn to compensate for the information loss occurring due to the fog.

**Scale Invariance & Fog Density :** Previously, LSE [Subhani and Ali, 2020] introduced scale-invariant examples in the target dataset to minimize the inconsistency between normal and larger scales. More specifically, they observed that in clear weather conditions, images at normal scale are segmented well instead of larger scale and hence they generated pseudo-labels at normal scale. However, in dense foggy scenes, this hypothesis is not completely true. In foggy scenes, resizing results in different segmentation accuracy at different locations of the input image depending upon the density of fog and how far or near the object is from the camera. This is especially true for the road scenes. Due to fog, the objects that are far from the camera (and hence smaller in scale) have lower visibility, (Eq. 1) making it further challenging to segment it correctly. Since we are employing a self-supervised training approach, pseudo-labels for the small and far away objects disguised in fog will thus not be available as they will have low segmentation scores. Therefore, we propose a scale-invariant pseudo-labels generation process for foggy scenes adaptation by exploiting the relationship between scale, fog, and self-entropy (Fig. 3). We make a reasonable assumption that

pseudo-labels should be scale-invariant. Using the same source trained model, the input target image is segmented at multiple image scales (higher and lower spatial resolution than original) independently and the output probability volume is aggregated. Segmenting at large scale extrapolates the local context and hence produces better segmentation and low entropy for faraway dense foggy regions compared to normal scale. Similarly, segmenting at small scale benefits large and near to camera objects disguised by fog as shown in Fig. 3. The combined effect of these three scales produces better pseudo-labels compared to single normal scale as shown later in Table. 6.

To summarize, this work produces the following contributions.

1. A self-supervised domain adaptation strategy for foggy scenes segmentation with pixel-level pseudo-labels to adapt the output space.
2. Exploiting relationship between the image scale and fog-density to design a strategy for generating *scale invariant* pixel-wise pseudo-labels.
3. Based on empirical evidence, defining a relation between fog density and self-entropy, i.e., self-entropy minimization loss to mitigate the effects of dense fog in segmentation model and produce confident segmentation output.
4. State-of-the-art (SOTA) performances on benchmark datasets by augmenting the scale invariance and self-entropy with *spatial distribution priors* of the source dataset.

The rest of the paper is arranged as follows: Section 2. describes related work. Section 3. details the proposed approach and Section 4. presents the experiments and results. In Section 5. we summarize our work for the conclusion.

## 2. RELATED WORK

Domain adaptation approaches have been presented to overcome the domain shift specific to the case of semantic segmentation [Tsai et al., 2018, Zou et al., 2018, Vu et al., 2019a, Iqbal and Ali, 2020a]. However, very little attention has been devoted to address domain shift caused by foggy weather conditions [Sakaridis et al., 2018b, Sakaridis et al., 2018a, Dai et al., 2019]. Below, we

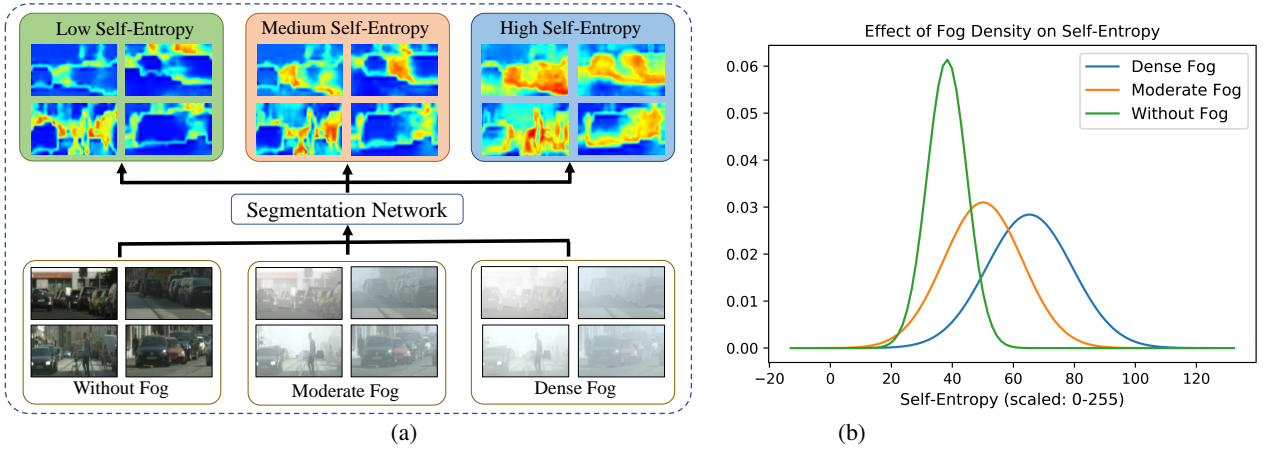


Figure 2: Relationship between fog density and uncertainty measured by self-entropy in segmentation probabilities. (a) Self-entropy maps of semantic segmentation computed over same images as fog changes from none to dense. Denser the fog, higher the self-entropy. (b) shows the self-entropy distributions for dense, moderate, and without fog image patches. The mean self-entropy increases with increasing fog density. (The visualizations are generated using a GTA dataset trained model, and for better visualization image-patches are shown instead of full images.).

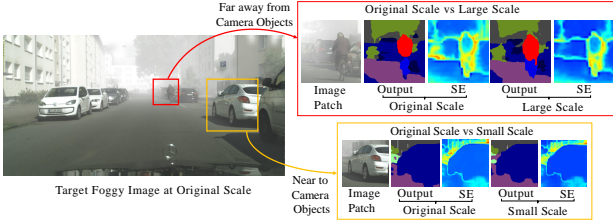


Figure 3: If an object is far or near the camera, resizing the foggy input image has a different effect on the self-entropy map. Segmenting foggy scenes at a higher scale provides extra local context, i.e., minimizes the effect of fog by producing better segmentation with comparatively sharp edges. Contrary to that, segmenting images at a lower scale produce better outputs for large and near to camera objects disguised by fog.

provide a succinct review of schemes related to generic domain adaptation for Semantic Segmentation followed by the schemes specific to Domain Adaptation for Foggy Scenes Segmentation.

## 2.1 Domain Adaptation for Semantic Segmentation

Adversarial learning based UDA of semantic segmentation is the most explored approach in literature [Kim and Byun, 2020, Zhang et al., 2018a, Kim et al., 2019, Gong et al., 2019, Chen et al., 2018b]. In UDA, adversarial loss-based training is leveraged for input space adaptation (re-weighting) [Zhang et al., 2018b, Hoffman et al., 2018], feature matching [Iqbal and Ali, 2020b, Chang et al., 2019, Chen et al., 2017, Mancini et al., 2018, Sankaranarayanan et al., 2018], structured output matching [Tsai et al., 2018, Vu et al., 2019a, Kim et al., 2019] or combination of these strategies [Kim et al., 2019, Vu et al., 2019b, Zhang et al., 2018a]. However, due to the global nature of adversarial learning even if the objective is to match the output probabilities or the high dimensional feature representation at latent space, the adversarial domain adaptation alone produces sub-optimal results [Vu et al., 2019a, Kim et al., 2019, Iqbal and Ali, 2020b].

Besides adversarial learning, self-supervised domain adaptation is gaining attention for many computer vision applications [Zou et al., 2018, Iqbal and Ali, 2020a, Khodabandeh et al., 2019]. The authors in [Zou et al., 2018, Zou et al., 2019] presented a class balanced pseudo-labels generation and confidence regularized self-

training with class spatial priors. The authors in MLSE [Iqbal and Ali, 2020a] leveraged spatial invariance to generate consistent pseudo-labels at pixels and image level for UDA of semantic segmentation in clear-weather scenes. LSE [Subhani and Ali, 2020] tried to generate scale-invariant examples and minimized the loss between pseudo-labels generated at normal scale and its zoomed version. Compared to proposed FogAdapt, the LSE [Subhani and Ali, 2020] and MLSE [Iqbal and Ali, 2020a] do not exploit multi-scale information during pseudo-label generation, hence producing inferior performance when exploited to foggy scenes. Zhang et al. [Zhang et al., 2019] proposed a curriculum domain adaptation by defining land-mark super-pixels classification based loss at the output while addressing the easy examples first. PyCDA [Lian et al., 2019] combined [Zou et al., 2018] and [Zhang et al., 2019] in a single framework to generate pseudo-labels at multiple sized windows. The authors in [Vu et al., 2019a] used a direct entropy minimization (only high entropy pixels) approach along with the adversarial learning applied on the self-entropy maps of the semantic segmentation.

## 2.2 Domain Adaptation for Foggy Scenes Segmentation

**2.2.1 Image Defogging/Dehazing** Color quality and contrast of the outdoor scenes are degraded due to the fog/haze. There have been many classical [He et al., 2010, Kim et al., 2011, Kim et al., 2013, Ancuti and Ancuti, 2014] and deep learning [Chen et al., 2019, Morales et al., 2019, Golts et al., 2019, Du and Li, 2018, Kim et al., 2019, Liu et al., 2019] based methods trying to improve color quality or contrast enhancement with an attempt to defog or dehaze. However, as the fog density increases, the defogging models' performance is degraded significantly. Therefore, attempt to use them as pre-processing step before feeding to computer vision models created/trained in normal light settings does not provide desired performance enhancement [Pei et al., 2018].

**2.2.2 Foggy Scenes Segmentation and Adaptation** Besides the great progress for generic semantic segmentation and domain adaptation, very little attention is being devoted to handle foggy scenes. This is mainly due to the unavailability of annotated datasets for foggy scene segmentation. The authors in [Sakaridis et al., 2018a] leveraged the stereo property of Cityscapes images to estimate the depth and proposed a fog simulation method for real imagery. They tried to add synthetic fog to real Cityscapes

images at multiple fog density levels defined by Eq. 2 to generate synthetic fog added real images with multiple visibility ranges (Fig. 1). Alongside, they also developed a small annotated dataset having real foggy scenes; *Foggy Driving*. Further, they fine-tuned the normal Cityscapes trained model on Foggy-Cityscapes images to address foggy scenes in real imagery. Similarly, the authors in [Hahner et al., 2019] tried to address the real foggy scenes segmentation problem with the help of purely synthetic foggy data. They fine-tuned the normal cityscapes trained models on the synthetic foggy images. Sakaridis et al. [Sakaridis et al., 2018b, Dai et al., 2019] proposed a curriculum adaptation learning approach for real foggy scenes understanding. They developed a large dataset, *Foggy Zurich*, by capturing road driving scenes under real foggy scenarios. The dataset is unlabeled except a small chunk of 40 images that have dense annotations available. They adapted to *Foggy Zurich* alongside the fully labeled Foggy-Cityscapes images. They generated pseudo-labels for target images using [Sakaridis et al., 2018a] and defined a fog estimator for curriculum learning. However, they did not investigate the effect of fog and induced uncertainty due to fog during adaptation.

In summary, the existing solutions for foggy scenes adaptation have multiple shortcomings. The generic adaptation methods fail to perform in foggy conditions due to lack of domain knowledge. The fog-specific approaches proposed in [Sakaridis et al., 2018a, Hahner et al., 2019, Sakaridis et al., 2018b, Dai et al., 2019] do not specifically investigate the effect of fog density and respectively induced uncertainty. Besides, we introduce a self-supervised domain adaptation approach for foggy scenes by exploiting the relationships between fog density and uncertainty and scale invariance.

### 3. APPROACH

In this section, we present the details of the proposed approach for self-supervised domain adaptation of semantic segmentation model for dense foggy scenes. We start with an introduction to the optical model for fog, basic architecture for semantic segmentation [Wu et al., 2019] and self-training method for domain adaptation [Zou et al., 2018, Iqbal and Ali, 2020a]. Next, we present the proposed FogAdapt algorithm including the loss functions.

#### 3.1 Optical Model for Fog

In general, the image fogging/hazing process is often represented as the physical corruption model given by Eq. 1 [Sakaridis et al., 2018a]

$$I_d(r, c) = J(r, c) t(r, c) + A(1 - t(r, c)), \quad (1)$$

where  $I_d$  is degraded image,  $t$  is the transmittance map,  $J$  is the fog-free radiance of the original image and  $A$  represents the global atmospheric lighting ( $(r, c)$  in Eq. 1 shows the pixel locations). The transmittance map  $t$  is dependent on the distance  $l(r, c)$  of the observer from the object having a homogeneous medium and is given by Eq. 2,

$$t(r, c) = \exp(-\beta l(r, c)). \quad (2)$$

The parameter  $\beta$  is used to control the density of fog as leveraged by [Sakaridis et al., 2018a]. Compared to daylight imagery with clear weather conditions, the foggy scenes are more challenging. As highlighted earlier, extensive research has been done on image defogging/dehazing, while less attention is being paid to foggy scenes segmentation and adaptation.

#### 3.2 Self-Supervised Domain Adaptation: Preliminaries

Let  $X_s \subset \mathbb{R}^{H_s \times W_s \times 3}$  and  $X_t \subset \mathbb{R}^{H_t \times W_t \times 3}$  be source domain (clear weather) and target domain (foggy) RGB images with spatial resolution  $H_s \times W_s$  and  $H_t \times W_t$  respectively. The true segmentation labels for source domain images are denoted by  $y_s \subset \mathbb{R}^{H_s \times W_s \times C}$  (each pixel location is one-hot encoded) while the ground truth labels for target images are not available.  $C$  is total number of classes. Let  $\mathcal{F}$  be the fully convolutional semantic segmentation model, with trainable parameters  $\theta$ . For a given source image  $x_s \in X_s$ , let the output segmentation probability volume be denoted by  $P_{x_s}$ . For source domain images, the segmentation model is trained using the cross entropy loss defined in Eq. 3,

$$\mathcal{L}(x_s, y_s) = - \sum_{h_s \in H_s} \sum_{w_s \in W_s} \sum_{c \in C} y_s(h_s, w_s, c) \log(P_{x_s}(h_s, w_s, c)) \quad (3)$$

where  $y_s \in Y_s$  shows the corresponding ground-truth segmentation labels. Since the true labels for target domain images are not present, we use pseudo-labels generated by the source domain trained model for fine-tuning (adaptation). The corresponding cross entropy loss for the target images is defined in Eq. 4,

$$\hat{\mathcal{L}}(x_t, \hat{y}_t) = - \sum_{h_t \in H_t} \sum_{w_t \in W_t} \sum_{c \in C} \rho(h_t, w_t) \hat{y}_t(h_t, w_t, c) \log(P_{x_t}(h_t, w_t, c)) \quad (4)$$

where  $\hat{\mathcal{L}}(x_t, \hat{y}_t)$  is self-supervised training loss for target domain images with pseudo-labels  $\hat{y}_t$ . The  $\rho^{(H_t, W_t)}$  is a binary map used to compute and backpropagate loss for only those pixels which are assigned pseudo-labels and ignore otherwise. More specifically, for any pixel location,  $\rho(h_t, w_t) = 1$  if that pixel is assigned a pseudo-label and  $\rho(h_t, w_t) = 0$  otherwise. The pseudo-labels generation and training processes for FogAdapt are shown in Fig. 4 (Sec. 3.3). During target adaptation, the segmentation network is jointly trained using the generated pseudo-labels of the target images and the ground truth labels of source images. The corresponding joint loss function for self-supervised domain adaptation (SSDA) is given by

$$\min_{\theta} \mathcal{L}_{SSDA}(x_s, y_s, x_t, \hat{y}_t) = \mathcal{L}(x_s, y_s) + \hat{\mathcal{L}}(x_t, \hat{y}_t) \quad (5)$$

The  $\mathcal{L}_{SSDA}$  in Eq. 5 is minimized following a sequential scheme, i.e., fix the segmentation model weight  $\theta$  to generate pseudo-labels  $\hat{y}_t$  for target samples  $x_t$ , and then use these pseudo-labels to minimize Eq. 5 with respect to  $\theta$ . These steps are repeated for multiple iterations called *rounds*. The pseudo-labels generation exploiting scale invariance and other constraints are discussed below.

#### 3.3 Scale Invariant Pseudo-Labels

To adapt the target domain effectively, accurate pseudo-labels are required. However, in dense foggy scenes, it is very difficult to generate accurate and consistent pseudo-labels. As described in Fig. 3 and explained in Section 1., under dense foggy conditions, image regions behave differently at multiple scales. Hence, combining multi-scale output information intelligently (Fig. 4(a)) is more effective compared to any single scale (Table. 6). Therefore, we present scale-invariant pseudo-labels created by weighted summation of the probability and uncertainty maps across different image scales.

As discussed in Section 1. and shown in Fig. 1, in foggy scenes the visibility of the object is correlated with density of

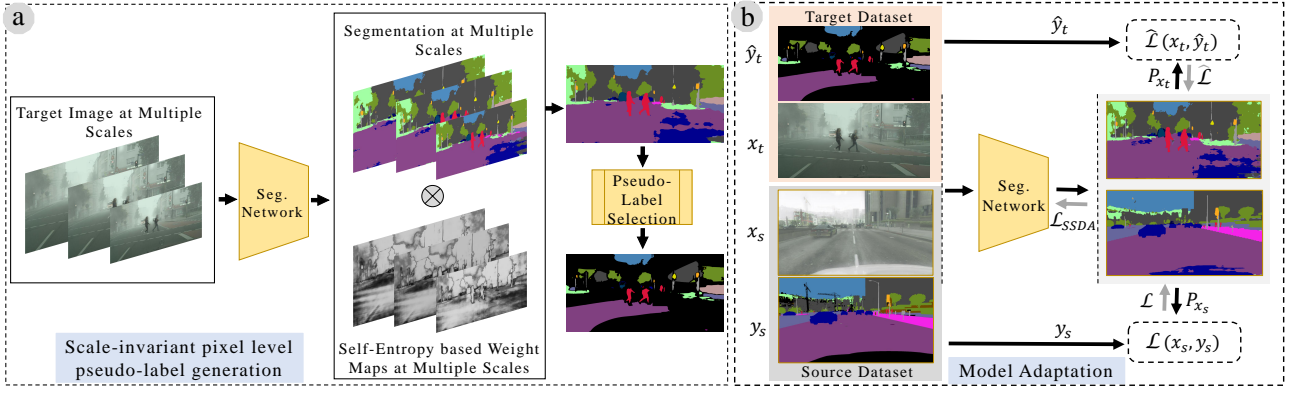


Figure 4: The proposed FogAdapt framework. (a) Scale-invariant pseudo-labels generation process where, 1) a target image is resized at multiple scales. 2) the resized versions of the image are segmented independently, 3) uncertainty (self-entropy) based weight maps for each image scale are defined and the outputs are weighted respectively 4) the weighted outputs are then resized to the original scale and recombined, and 5) most confident pixels are assigned pseudo-labels. (b) shows the semantic segmentation adaptation using the generated pseudo-labels for target domain images in (a) and the true labels of source domain images simultaneously.

fog present, and the distance between an object and the sensor. The combined effect of these deteriorates the performance of the semantic segmentation model. Pixels of the faraway and near to camera objects camouflaged in fog presents very limited information. More specifically, the model trained on clear weather images skip out small and washed-out content with respect to available large neighboring content-generating merged or inferior segmentation output. Similarly, due to the limited receptive field of the segmentation model compared to large and near to camera objects, i.e., bus, truck etc., the performance is effected negatively. Segmentation model might be relying on texture or structure information to make the decision. However, that information is corrupted by the presence of the fog, resulting in the decreased confidence for these parts and hence fewer pseudo-labels for it.

To minimize the effect of dense fog on far away objects and to overcome the problems associated with the fixed receptive field being unable to provide the complete coverage to larger and near to camera objects, we generate scale-invariant pseudo-labels. Instead of generating pseudo-labels at the original (normal) scale that objects exist in an image, we process target images at multiple scales (spatial resolutions/zoom levels) to generate pseudo-labels, as shown Fig. 4(a). To assure semantic consistency and scale-invariance, we assume that objects and stuff should be segmented the same irrespective of the scale they are presented. We evaluate the target image at three scales, e.g.,  $S = \{1 + s_c, 1, 1 - s_c\}$ , where  $s_c$  is a scale parameter and set to  $s_c = 0.25$  in this work. The target image is resized according to the three scale parameters into three separate images and segmented independently. We combine these probability maps based on the confidence of the segmentation model. Specifically, corresponding to each scale, we generate normalized weight maps ( $w_{(1-s_c)}$ ,  $w$  and  $w_{(1+s_c)}$ ) based on the self entropy  $\mathcal{H}^{(H_t, W_t)}$  (Eq. 8) of the segmentation probabilities corresponding to each scale. This process for  $w_{(1-s_c)}$  is shown in Eq. 6.

$$w_{(1-s_c)} = \frac{1 - \mathcal{H}^{(H_t, W_t)}(P_{x_{(1-s_c)}})}{\sum_{j \in S} (1 - \mathcal{H}^{(H_t, W_t)}(P_{x_j}))} \quad (6)$$

where  $j \in S$  represents the image scale. Similar equations can be written for  $w$  and  $w_{(1+s_c)}$ . Using these weight maps, we obtain a weighted summation after resizing to normal scale to form  $P_{x_c} \in \mathbb{R}^{H_t \times W_t \times C}$ .

$$P_{x_c} = \sum_{j \in S} w_j \cdot P_{x_j} \quad (7)$$

where  $w_j$  with  $(j \in S)$  are the self-entropy based weight maps for respective scales and the  $(\cdot)$  operator shows element-wise multiplication. The higher the self-entropy, the lower the contribution in  $P_{x_c}$  and vice versa. The  $P_{x_c}$  is used to select pseudo-label based on the confidence score. This process of scale-invariant pseudo-label generation is shown in Fig. 4(a). Hence, the generated pseudo-labels are scale-invariant and quantitatively better compared to single inference (Table. 6).

To select pixels with high confidence as pseudo-labels and avoid class distribution imbalance problem, we adapt a class balancing and selecting criteria similar to one used in [Zou et al., 2019]. For each target image, we select the per-pixel high (maximum) probability values from the probability map  $P_{x_c}$ . These high-probability class values over the whole target set are sorted in descending order of confidence and the pixels with high probabilities are selected as pseudo-labels based on the pre-defined selection portion  $s_p$ . Initially,  $s_p = 15\%$  of the total pixels belonging to any category and is incremented by 5% in each round. The resultant pseudo-labels are class-balanced, consistent, and scale-invariant representative of the whole target dataset.

### 3.4 Self-Entropy Minimization for Foggy Scenes Adaptation

The density of fog has a direct relation with the information contained in an image, e.g., the denser the fog, the minimum the information. This is evident from the semantic segmentation results, where dense foggy regions in an image have high self-entropy values (Fig. 2). With increasing fog density, the segmentation model generates under-confident per-pixel predictions making the entropies high. We leverage this relationship between fog density and self-entropy and define a self-entropy minimization loss (9) alongside cross-entropy loss (5). The underlying idea for self-entropy minimization is to shift the mean self-entropy of dense foggy scenes towards clear images self-entropy mean, as shown in Fig. 2 (b). The self-entropy  $\mathcal{H}$  for a target image  $x_t$  is given by Eq. 8,

$$\mathcal{H}^{(H_t, W_t)}(P_{x_t}) = -\frac{1}{\log(C)} \sum_{c \in C} P_{x_t}^{(H_t, W_t, c)} \log(P_{x_t}^{(H_t, W_t, c)}) \quad (8)$$

where  $\mathcal{H}^{(H_t, W_t)} \in [0, 1]$  is the per-pixel standard entropy defined in [Shannon, 1948]. The loss function based on  $\mathcal{H}$  for a

target image  $x_t$  is given by Eq. 9,

$$\hat{\mathcal{L}}_{se}(P_{x_t}) = \frac{1}{H_t \times W_t} \sum_{H_t, W_t} \mathcal{H}^{(H_t, W_t)}(P_{x_t}^{(H_t, W_t, c)}) \quad (9)$$

During adaptation, we jointly optimize the pseudo-labels based supervised loss  $\hat{\mathcal{L}}$  and the unsupervised self-entropy loss  $\hat{\mathcal{L}}_{se}$  for an input target image  $x_t$ . There is a strong resemblance in Eq. 4 and Eq. 9, where the former enforces the segmentation model to assign the correct class to an underlined pixel, while the later tries to maximize individuals confidence scores.

### 3.5 Appearance Adaptation

As described in Section 2., many algorithms tried to exploit the self-training process by labeling the most confident predictions as pseudo-labels. However, it is very important for a pseudo-label to be accurate, consistent, and invariant. To generate such confident pseudo-labels the visual appearance of the target and source domain images also play a vital role. For example, a model trained on normal imagery fails to generate accurate pseudo-labels on dense foggy images. Hence, an appearance adaptation step is required to help self-supervised learning paradigms to generate consistent pseudo-labels.

**3.5.1 Image Translation Module** In this work, we leveraged the cycle-consistent adversarial learning algorithm (CycleGAN) [Hoffman et al., 2018] to transform the source domain images to the visual appearance of the unlabeled target domain images. This process is named as Image Translation Module (ITM). The transformed images are nearly similar in visual appearance with target domain images and are used in the domain adaptation process. The loss function for the employed CycleGAN is given by Eq. 10,

$$\begin{aligned} \mathcal{L}_{c-Gan}(x_s, x_t, G_t, G_s, D_t, D_s) = & \mathcal{L}_{GAN}(G_t, D_t, x_s, x_t) \\ & + \mathcal{L}_{GAN}(G_s, D_s, x_t, x_s) + \mathcal{L}_{cyc}(x_s, G_s(G_t(x_s))) \\ & + \mathcal{L}_{sc}(x_s, G_t(x_s)), \end{aligned} \quad (10)$$

where  $G_s$  and  $G_t$  represent the generator from target to source and source to target domain respectively.  $D_t$  is the discriminator applied to classify between original target domain images and translated target domain images.  $D_s$  expedites the same loss for the target to source transformation. Similarly,  $\mathcal{L}_{cyc}$  and  $\mathcal{L}_{sc}$  losses are applied to maintain the cycle and semantic consistency respectively. The optimization program can be defined as a min-max criterion given in Eq. 11,

$$\min_{G_t, G_s} \max_{D_t, D_s} \mathcal{L}_{c-Gan}(x_s, x_t, G_t, G_s, D_t, D_s). \quad (11)$$

The transformed source images with available ground truth, when used in domain adaptation helps to select better pseudo-labels and eventually improves the adaptation performance.

### 3.6 Combined Objective Function

The composite loss function for self-supervision based UDA of foggy scene segmentation is the composition of both Eq. 5 and Eq. 9, and is given by,

$$\mathcal{L}_{cmp}(x_s, y_s, x_t, \hat{y}_t, c) = \mathcal{L}_{SSDA}(x_s, y_s, x_t, \hat{y}_t) + \hat{\mathcal{L}}_{se}(P_{x_t}) \quad (12)$$

Similarly, the combined loss function for ITM augmented with  $\mathcal{L}_{cmp}$  is the combination of Eq. 10 and Eq. 12 and is given by Eq. 13,

$$\begin{aligned} \mathcal{L}_{ITM-cmp} = & \mathcal{L}_{c-Gan}(x_s, x_t, F_t, F_s, D_t, D_s) \\ & + \mathcal{L}_{cmp}(x_s, y_s, x_t, \hat{y}_t, c). \end{aligned} \quad (13)$$

To summarize the proposed approach, we train CycleGAN using Eq. 11 to translate source images to look alike target images. Next, we generate scale-invariant consistent pseudo labels and adapt the baseline model in an iterative manner to minimize the loss function  $\mathcal{L}_{cmp}$  defined in Eq. 12.

## 4. EXPERIMENTS AND RESULTS

This section discusses experimental details and provides the results of our comparison with the state of art techniques. We list down different configurations and their acronyms in Table. 1 for better readability.

Table 1 Different configurations and their acronyms.

Acronyms	Configuration
FogAdapt	Self-entropy loss + Scale-invariance based pseudo-labels
FogAdapt+	ITM (Image Translation Module) + FogAdapt
SP-FogAdapt+	Spatial-Priors during pseudo-labels generation + FogAdapt+

### 4.1 Experimental Setup

We have performed multiple experiments with various datasets, weather conditions and settings. The key points are discussed below.

**4.1.1 Datasets** We adapt the standard *real-to-real* and *synthetic-to-real* setup for UDA of foggy scenes segmentation. We use Cityscapes [Cordts et al., 2016], SYNTHIA [Ros et al., 2016] and, GTA [Richter et al., 2016] datasets as source domain and *Foggy Driving* [Sakaridis et al., 2018a], *Foggy-Cityscapes* [Sakaridis et al., 2018a] and foggy zurich [Dai et al., 2019] as real-world target domain datasets. The SYNTHIA-RAND-CITYSCAPES, a sub-set from the SYNTHIA dataset consists of 9400 synthetic frames of spatial resolution  $760 \times 1280$ . The baseline models and the adapted models are both evaluated with 16 and 13 categories common between SYNTHIA and Foggy-Cityscapes as described in [Vu et al., 2019a] and [Zou et al., 2018] for normal Cityscapes. Similarly, we use the GTA dataset having 24966 frames with a high spatial resolution of  $1052 \times 1914$ . Pixel-level labels for classes compatible with Foggy-Cityscapes are available for all 24966 frames. The Cityscapes dataset consists of 3475 high resolution ( $1024 \times 2048$ ) images with pixel-level annotations, where 2975 images are listed as the training set and the remaining 500 as validation. The Foggy-Cityscapes have the same images as cityscapes with fog being added synthetically by [Sakaridis et al., 2018b]. The *Foggy Driving* (FD) dataset contains 101 images where 33 images have fine annotations and the remaining have coarse labels available. *Foggy Driving Dense* FDD is a subset of the FD dataset having 21 images with very dense fog. Similarly, the *Foggy Zurich* dataset contains 3808 high-resolution images of real foggy scenes. However, only a limited set of 40 images is labeled for semantic segmentation.

**4.1.2 Model Architecture** For semantic segmentation of foggy scenes, we use ResNet-38 [Wu et al., 2019] as baseline. The ResNet-38 is trained for segmentation of Cityscapes, SYNTHIA, and GTA datasets using the ImageNet trained parameters [Russakovsky et al., 2015]. The architecture of ResNet-38 for segmentation in this work is the same as defined in [Wu et al., 2019, Zou et al., 2018]. The Image Translation Module (ITM) is adapted from [Hoffman et al., 2018]. The ITM is employed to translate source images to the visual appearance of the target domain datasets, e.g., from GTA to Foggy-Cityscapes.

Table 2 Semantic segmentation performance of **FogAdapt** and its variants compared to SOTA methods on *Foggy Zurich* (FZ), *Foggy Driving-dense* (FDD) and *Foggy Driving* (FD) test sets when **adapted from Cityscapes to FZ**. We present mIoU for all classes compatible with Cityscapes [Cordts et al., 2016], and frequent classes defined for FZ, FDD, and FD respectively. FogAdapt+: FogAdapt+CycleGAN, **SP-FogAdapt+**: FogAdapt+ combined with spatial priors defined in [Zou et al., 2018]. The **bold** text shows highest whereas the underlined show the second-highest scores.

Dataset Methods	IoU over all Classes			IoU over frequent Classes		
	FZ	FDD	FD	FZ	FDD	FD
AdaptSegNet [Tsai et al., 2018]	25.0	15.8	29.7	-	-	-
Semantic [Sakaridis et al., 2018a]	-	-	37.8	-	-	57.4
Curriculum-FT [Dai et al., 2019]	36.7	-	-	51.7	-	-
SUSF [Hahner et al., 2019]	42.7	-	48.6	63.0	-	59.5
Model-Ada [Sakaridis et al., 2018b]	42.9	37.3	48.5	-	-	-
MLSL [Iqbal and Ali, 2020a]	45.5	43.3	43.5	61.0	46.5	58.8
Curriculum-Ada [Dai et al., 2019]	46.8	43.0	49.8	-	-	-
ResNet-38 (baseline) [Wu et al., 2019]	33.8	39.2	39.4	48.0	43.9	56.6
Ours(FogAdapt)	48.8	46.5	52.0	64.2	51.1	63.5
Ours(FogAdapt+)	49.8	47.1	52.4	64.4	51.6	63.7
Ours( <b>SP-FogAdapt+</b> )	<b>50.6</b>	<b>49.0</b>	<b>53.4</b>	<b>64.6</b>	<b>53.1</b>	<b>65.7</b>

**4.1.3 Implementation and Training Details** To perform the experiments, a core-i5 machine with a single GTX-1080Ti having 11GB of memory is used while MxNet [Chen et al., 2015] is used as deep learning framework. SGD optimizer with an initial learning rate of  $1 \times 10^{-4}$  for the segmentation model and  $2 \times 10^{-4}$  for ITM respectively are used for training. To enforce scale-invariance, the images are segmented at three scales to generate pseudo-labels, e.g.,  $S = \{1 + s_c, 1, 1 - s_c\}$ , where  $s_c$  is a scale parameter and is set to  $s_c = 0.25$  in this work. Similarly,  $s_p$  is initially set to 15% of the total pixels belonging to any category for pseudo-labels selection and is incremented by 5% in each round (Sec. 3.3). Due to GPU memory limitations, we process two images per mini-batch. The proposed (FogAdapt) iterative process of self-supervised domain adaptation is continued for 4 rounds where each round consists of 2 epochs of training.

## 4.2 Experimental Results

In this section, we show and discuss the experimental results of the **FogAdapt** compared to ResNet-38 (baseline) and current state-of-the-art (SOTA) UDA approaches for foggy scenes. Our experiments are two fold: a) In the first setup, we use normal *Cityscapes* (clear-weather images) dataset as source domain and *Foggy Zurich* and *Foggy Driving* (real-foggy imagery) as target domain datasets and (b) in the second setup, we use synthetic datasets, e.g., *SYNTHIA* and *GTA* as source domain and *Foggy-Cityscapes* (synthetic fog added to real images) dataset as target domain. The performance is reported using a standard evaluation metric for segmentation, i.e., Mean Intersection over Union (mIoU). The proposed FogAdapt performs superior compared to other domain adaptation approaches with SOTA performance on multiple benchmark datasets varying from synthetic to real for dense foggy conditions.

### 4.2.1 Real Non-foggy to Real-Foggy Scenes Adaptation

Following [Sakaridis et al., 2018b, Dai et al., 2019], we adapt the normal (clear-weather) cityscapes dataset trained source model to real foggy imagery dataset, *Foggy Zurich*. Alongside *Foggy Zurich* evaluation set, we also evaluate our baseline and *Foggy*

*Zurich* (FZ) adapted model over *Foggy Driving* (FD) and *Foggy Driving-dense* (FDD) datasets.

**Cityscapes → Foggy Zurich:** Table. 2, summarizes the quantitative results of the proposed approach compared to current SOTA methods. The proposed FogAdapt+ outperforms the ResNet-38 (baseline) and existing approaches with a high margin. Compared to ResNet-38 [Wu et al., 2019] baseline, we gain 16.0% in mIoU over all classes. We also evaluate FogAdapt over frequent classes in the FZ dataset, e.g., *road*, *sidewalk*, *building*, *wall*, *fence*, *pole*, *traffic-light*, *traffic-sign*, *vegetation*, *sky*, and *car* defined by [Dai et al., 2019]. The FogAdapt+ attains a gain of 22.4% in mIoU over ResNet-38 baseline. Similarly, compared to Curriculum-Ada [Dai et al., 2019] and Model-Ada [Sakaridis et al., 2018b], the proposed FogAdapt+ outperforms with significant margins of about 3.0% and 7.0% over all classes respectively. The addition of spatial priors further improves the results as shown by **SP-FogAdapt+** in Table. 2. To have a fair qualitative comparison, we selected the same images presented in [Dai et al., 2019] as shown in Fig. 5. The proposed FogAdapt shows a significant performance improvement over baselines and existing SOTA methods in most of the categories.

**Evaluation on Foggy Driving:** Since the FD dataset is small having 33 images with fine (every pixel is assigned a label) dense annotations and the remaining 68 images with coarse (polygon annotations with no clear object boundaries) annotations, this dataset is used only for evaluation as suggested by [Sakaridis et al., 2018a]. We evaluate our baseline and FZ adapted models over FD and its' subset FDD. The quantitative results for all 19 classes compatible with FZ dataset are shown in Table. 2. The proposed FogAdapt+ performs superior compared to baselines and existing SOTA methods. Especially, in case of dense foggy scenes, FDD, our FogAdapt+ achieves a gain of 4.1% and 9.8% in mIoU compared to Curriculum-Ada [Dai et al., 2019] and Model-Ada [Sakaridis et al., 2018b] respectively.

Similar to the FZ dataset, we evaluate the FD dataset for frequent classes, e.g., *road*, *sidewalk*, *building*, *pole*, *traffic-light*, *traffic-sign*, *vegetation*, *sky*, *person*, and *car* as defined by [Sakaridis et al., 2018a]. The proposed FogAdapt+ performs significantly better in mIoU, i.e., a minimum gain of 5.1% compared to strong MLSL [Iqbal and Ali, 2020a].

**4.2.2 Synthetic to Real-Foggy Scenes Adaptation** To comprehensively test the proposed approach, we also perform synthetic to real foggy domain adaptation experiments. Specifically, we use synthetic datasets, e.g., *SYNTHIA* and *GTA* as source domain datasets and *Foggy-Cityscapes* dataset as target domain. The *Foggy-Cityscapes* dataset has the real *Cityscapes* images with synthetic fog added as proposed by [Dai et al., 2019]. The *Foggy-Cityscapes* have three levels of fog, e.g., low fog with 600-m visibility, medium fog with 300-m visibility, and dense fog with 150m visibility (Fig. 1). In this work, we have adapted our models to dense fog scenarios of the *Foggy-Cityscapes* dataset.

**GTA → Foggy-Cityscapes:** As indicated in Table. 3, the proposed FogAdapt+ for self-supervised domain adaptation shows SOTA performance. More specifically, the FogAdapt+ improves the segmentation performance on dense *Foggy-Cityscapes* by 11.6%, 7.3% and 5.9% compared to ResNet-38 baseline and previous SOTA methods, i.e., CBST [Zou et al., 2018] and MLSL [Iqbal and Ali, 2020a] respectively. Similarly, compared to LSE [Subhani and Ali, 2020] and PyCDA [Lian et al., 2019], the proposed approach outperform with a minimum margin of 5.0%. Fig. 6 shows semantic segmentation results before and after adaptation. The proposed approach significantly improves the segmentation performance of dense foggy scenes compared to baseline and previous SOTA methods.

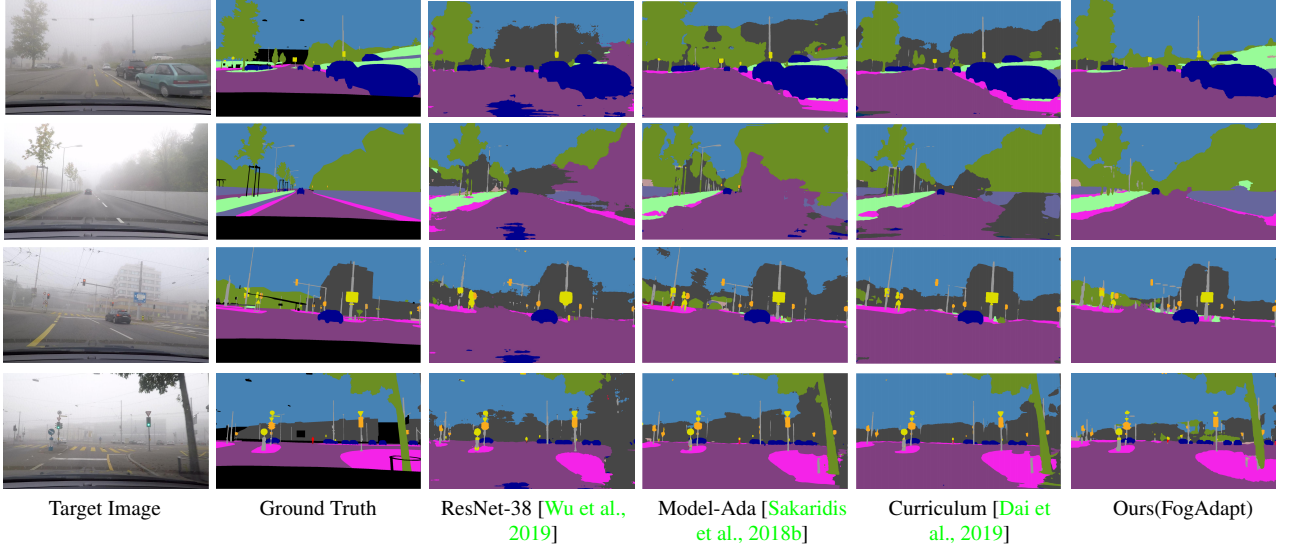


Figure 5: Segmentation results on *Foggy Zurich* test set when adapted from Cityscapes. For a fair comparison we, select the images shown by [Dai et al., 2019]. The proposed FogAdapt performs better in most of the classes ranging from road to vegetation, train, sky, wall and buildings.

Table 3 Segmentation results of adapting GTA to Foggy-Cityscapes. The abbreviations " $S_T$ ", " $A_I$ " and " $A_O$ " indicates the self-training (self-supervised domain adaptation), input space and output space adversarial learning respectively. PyCDA\* trained with 2 batch size instead of 8 ([Lian et al., 2019]) due to memory limitations.

GTA → Foggy-Cityscapes																					
Methods	Appr.	Road	Sidewalk	Building	Wall	Fence	Pole	T. Light	T. Sign	Veg.	Terrain	Sky	Person	Rider	Car	Truck	Bus	Train	Mcycle	Bicycle	mIoU
ResNet-38 [Wu et al., 2019]	-	69.5	12.9	65.6	10.5	6.8	39.5	41.7	20.4	62.7	7.5	63.5	58.5	31.1	62.3	16.3	31.9	1.4	22.0	10.8	33.4
BDL [Kim et al., 2019]	$A_O$	89.6	37.6	65.4	19.5	14.4	23.2	22.7	25.5	48.9	<u>35.7</u>	39.7	50.7	<u>29.8</u>	79.1	<b>27.9</b>	32.8	0.2	18.5	30.4	36.3
CBST [Zou et al., 2018]	$S_T$	74.6	30.3	73.2	7.0	20.0	40.7	47.4	35.4	53.0	5.8	65.4	47.7	21.7	75.4	21.7	<b>39.1</b>	5.5	18.5	33.5	37.7
MLSL [Iqbal and Ali, 2020a]	$S_T$	81.5	33.6	76.6	7.9	23.1	41.1	47.5	35.9	52.0	6.1	64.9	54.1	27.8	81.2	16.5	37.7	1.5	17.4	36.7	39.1
LSE [Subhani and Ali, 2020]	ST	81.9	29.0	73.3	20.7	23.2	29.1	36.9	32.7	70.4	13.4	60.9	54.8	<b>33.0</b>	75.9	25.1	27.7	7.1	25.4	33.2	39.7
PyCDA* [Lian et al., 2019]	$S_T$	80.9	23.7	72.4	17.2	<b>28.3</b>	27.1	38.4	17.6	<u>72.0</u>	<b>39.9</b>	<u>74.2</u>	<b>64.3</b>	<u>24.3</u>	72.4	<u>26.2</u>	19.1	0.6	24.2	36.9	40.0
Ours (FogAdapt)	$S_T$	<u>85.1</u>	31.7	<u>76.7</u>	16.5	20.3	41.2	46.2	34.9	70.8	9.1	63.8	<u>53.9</u>	26.2	81.5	22.0	<u>38.0</u>	5.9	19.0	36.3	41.0
Ours (FogAdapt+)	$S_T + A_I$	84.1	<u>37.5</u>	76.1	21.9	22.4	41.9	48.6	44.2	58.3	8.2	59.0	<u>58.9</u>	23.0	<b>81.9</b>	<b>26.0</b>	33.0	<u>9.3</u>	<b>31.1</b>	<u>40.0</u>	42.8
Ours (SP-FogAdapt+)	$S_T + A_I$	<b>89.6</b>	<b>41.0</b>	<b>77.7</b>	<u>22.6</u>	<u>24.7</u>	<b>42.0</b>	<b>49.9</b>	<u>47.7</u>	<b>80.3</b>	16.4	<u>68.7</u>	<u>50.2</u>	21.9	<u>81.6</u>	25.3	34.5	<b>10.7</b>	30.4	<b>40.5</b>	<b>45.0</b>

**SYNTHIA → Foggy-Cityscapes:** Compared to GTA and FoggyZurich, the SYNTHIA dataset has extra constraints like multiple viewpoint imagery making it a more difficult adaptation task. Table 4 presents the quantitative results of the proposed approach for 16 overlapping classes between SYNTHIA and Foggy-Cityscapes. Following [Tsai et al., 2018, Luo et al., 2019], we also show the 13 frequent classes results (mIoU\*). Compared to baseline ResNet-38, the proposed FogAdapt+ shows a gain of 18.9% and 20.8% in mIoU and mIoU\* respectively. Similarly, compared to bidirectional learning [Kim et al., 2019] (output space adversarial learning only), CBST [Zou et al., 2018] and MLSL [Iqbal and Ali, 2020a], FogAdapt+ shows a minimum gain of 3.9% and 4.4% in mIoU and mIoU\* respectively. A qualitative comparison of FogAdapt with existing SOTA methods is presented in Fig. 7

### 4.3 Discussion

This section investigates the effect of each part of the proposed approach and discusses it in relation to the results obtained.

**4.3.1 Self-Entropy Minimization** As discussed in Sec. 1., the higher the fog density, the more uncertain the segmentation model becomes about assigning a class to a specific pixel (Fig. 1). This decrease in information eventually increases the self-entropy of segmentation probabilities (Fig. 2). We leverage this relation between entropy and fog density and add an entropy minimization constraint (Eq. 9) to the total loss function. Adding this

constraint increases the mIoU performance compared to simple pseudo-labels based self-supervised domain adaptation (SSDA) further by 3.3% for GTA to Foggy-Cityscapes as shown in Table. 5.

Table 5 Effect of self-entropy and scale invariance. SSDA: Self-supervised domain adaptation. Here SE is Self-entropy while SI is Scale Invariance.

		GTA → Foggy-Cityscapes			
Methods	ResNet-38	SSDA	SSDA-SE	SSDA-SI	FogAdapt
mIoU	33.4	37.0	40.3	40.2	41.0

**4.3.2 Scale-Invariance** As the effect of fog increases with the distance between the object and the observer, the scale of an object has a major role (Fig. 3) in properly segmenting the object. Increasing the object's size by resizing the image to a larger scale makes the object under fog clearer as it increases the local contextual information (Fig. 3). This helps in generating comparatively better pseudo labels (Table. 6). On the other hand, resizing image to a smaller size allows the segmentation algorithm to properly segment near to camera objects disguised by fog which were erroneous previously due to limited receptive field, and capture a more global view. As described in Sec. 3.3, combining these higher and lower scales results in the generation of robust and consistent pseudo-labels (Table. 6), which eventually increases the performance over foggy scenes. Experimental results show

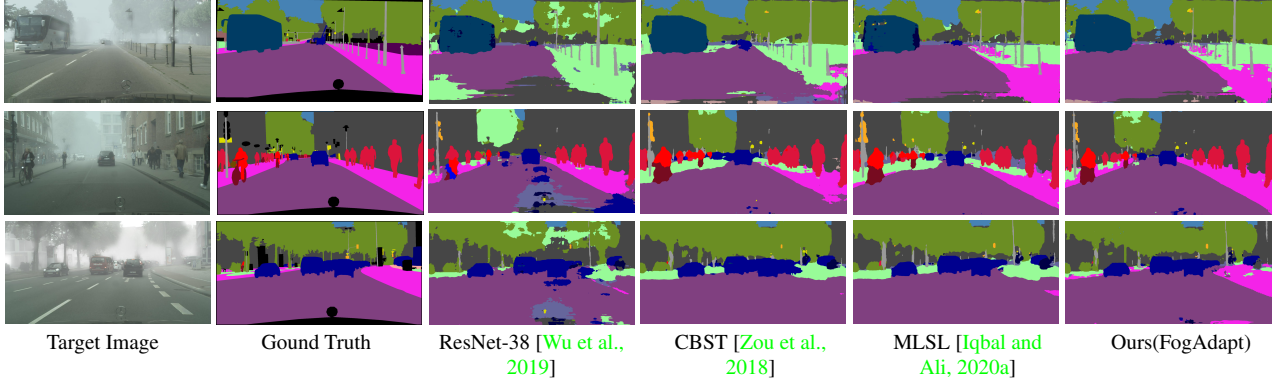


Figure 6: Semantic segmentation qualitative results on Foggy-Cityscapes validation set when adapted from GTA dataset trained model. The FogAdapt performs better compared to existing methods. Specifically, the small, thin and far away objects disguised in fog and the stuff classes like road, sidewalk, buildings and sky are segmented better.

Table 4 Segmentation results of adapting SYNTHIA to Foggy-Cityscapes. We present mIoU and mIoU\* (13-categories as presented by [Tsai et al., 2018]) on the Foggy-Cityscapes validation set.

SYNTHIA → Foggy-Cityscapes																			
Methods	Appr.	Road	Sidewalk	Building	Wall	Fence	Pole	T. Light	T. Sign	Veg.	Sky	Person	Rider	Car	Bus	Mcycle	Bicycle	mIoU	mIoU*
ResNet-38 [Wu et al., 2019]	-	29.3	21.3	34.5	0.8	0.0	17.5	15.8	8.2	17.1	33.5	57.1	4.7	71.2	12.2	2.9	8.9	20.9	24.4
BDL [Kim et al., 2019]	$A_O$	<b>83.2</b>	<b>43.2</b>	63.6	2.38	0.1	19.1	6.8	5.3	35.4	19.9	55.4	<b>31.8</b>	65.2	<b>21.0</b>	<b>27.6</b>	37.1	32.3	38.1
CBST [Zou et al., 2018]	$S_T$	70.5	31.2	<u>57.62</u>	2.9	0.02	31.7	29.1	23.1	38.5	41.1	61.3	18.9	75.0	8.3	11.9	32.1	33.3	38.4
MLSL [Iqbal and Ali, 2020a]	$S_T$	48.9	27.2	53.4	11.4	0.4	31.9	<b>32.4</b>	21.0	49.2	40.1	<b>65.8</b>	24.4	<b>77.8</b>	20.9	19.0	<b>50.5</b>	35.9	40.8
Ours (FogAdapt)	$S_T$	62.2	28.0	56.4	<u>13.1</u>	0.7	30.3	<u>30.1</u>	27.4	<u>61.7</u>	<b>61.8</b>	54.9	<u>30.0</u>	66.1	2.6	12.1	44.8	36.4	41.4
Ours (FogAdapt+)	$S_T + A_I$	68.3	<u>34.0</u>	<b>64.7</b>	<b>14.2</b>	<b>2.1</b>	<b>33.2</b>	28.7	<b>31.5</b>	<b>69.7</b>	<u>56.1</u>	<u>63.8</u>	29.1	66.3	6.0	<u>21.4</u>	<u>47.3</u>	<b>39.8</b>	<b>45.2</b>

a gain of 3.2% in mIoU compared to single scale for GTA to Foggy-Cityscapes adaptation (Table. 5). Similarly, for normal Cityscapes to FZ dataset adaptation, the SI performs superior when combined with SE for FZ, FDD, and FD compared to all previous approaches as shown in Table. 2 (FogAdapt+)).

Table 6 Effect of incorporating uncertainty weighted scale invariance on the quality of pseudo-labels. Here wSI is Weighted Scale-Invariance.

GTA → Foggy-Cityscapes				
Methods	Start of round 0		Start of round 1	
	Normal Scale	wSI based multi-scale	Normal Scale	wSI based multi-scale
mIoU	69.6	<b>71.5</b>	71.3	<b>74.3</b>

**4.3.3 Effect of Input Space Adaptation** With ResNet-38 [Wu et al., 2019] as baseline model, we investigate the effect of image translation at input space. We train CycleGAN [Hoffman et al., 2018] to translate source images (non-foggy) to the visual appearance (foggy) of the target domain images; GTA/SYNTHIA to Foggy-Cityscapes and Cityscapes to *Foggy Zurich* respectively. This process generates foggy imagery for the source datasets helping FogAdapt to generate better pseudo-labels. Adding image translation module with FogAdapt; FogAdapt+, significantly improves the segmentation performance for foggy scenes. For GTA to Foggy-Cityscapes, FogAdapt+ gains 1.8% in mIoU as shown in Table 3. Similarly, for normal Cityscapes to real foggy datasets adaptation the FogAdapt+ gain 1.0%, 0.5% and 0.4% in mIoU for FZ, FDD and FD over the FogAdapt respectively (Table. 2). Thus, the input space adaptation has an impact on the pseudo-label generation and adaptation process.

**4.3.4 Effect of Dehazing/Defogging** To investigate the effect of the defogging process, we conduct experiments with defogging as input space adaptation. We define an image defogging module (IDM) based on the method proposed by [Chen et al.,

2019]. FogAdapt is applied on these defogged images for domain adaptation. However, it is observed that defogging methods perform inferior in the presence of dense fog. The same observation was previously reported by [Dai et al., 2019]. Compared to defogging as input space adaptation, the source images translation to the target domain appearance performs well (Table. 7).

Table 7 A comparative analysis of image transformation methods in dense foggy scenes adaptation process.

GTA → Foggy-Cityscapes				
Methods	ResNet-38	FogAdapt	IDM-FogAdapt	ITM-FogAdapt
mIoU	33.4	41.0	40.0	42.8

## 5. CONCLUSION

In this paper, we have proposed a self-supervised domain adaptation strategy with self-entropy and scale-invariance constraints for UDA of foggy scene semantic segmentation. We empirically establish a relationship between the fog density and self-entropy of the source model’s prediction over the foggy images. We exploit this relationship to define a self-entropy minimization objective function to adapt on images where color quality and contrast has been degraded due to fog. Having a fair assumption that under foggy conditions labels of stuff and objects should be the same regardless of their scale, we generate scale-invariant pixel level pseudo-labels. Scale-invariance helps us to counter the phenomena that in foggy weather, objects farther away are less visible and hence suffer from more information loss. The scale invariant pseudo-label generation and the self-entropy minimization for self-supervised domain adaptation, allows the segmentation model to learn domain independent features to mitigate the effect of fog density. Rigorous experiments demonstrate that the proposed self-supervised domain adaptation method augmented with image translation module (ITM) outperforms the existing SOTA algorithms on benchmark datasets:

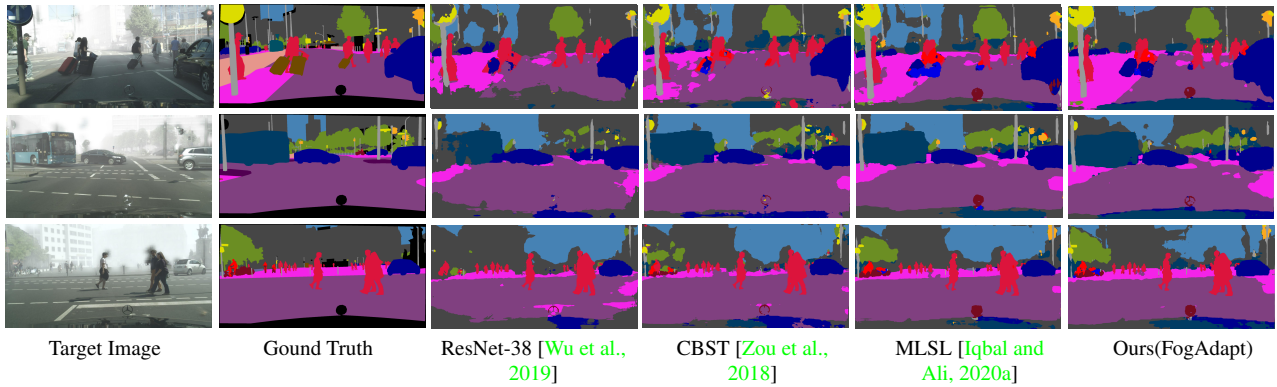


Figure 7: Qualitative results of semantic segmentation on Foggy-Cityscapes validation set when adapted from SYNTHIA dataset trained model. The proposed FogAdapt performs better compared to [Zou et al., 2018] and [Iqbal and Ali, 2020a].

mIoU improves from 46.8 to 50.6 on *Foggy Zurich*, 43.0 to 49.0 on *Foggy Driving-dense* and 49.8 to 53.4 *Foggy Driving* when adapted from Cityscapes to *Foggy Zurich*. Effectiveness of self-entropy minimization, scale invariant pseudo-labels, and ITM is highlighted by the considerable improvement of mIoU over the baseline model and SOTA methods.

## REFERENCES

- Ancuti, C. and Ancuti, C. O., 2014. Effective contrast-based dehazing for robust image matching. *IEEE Geoscience and Remote sensing letters* 11(11), pp. 1871–1875. [3](#)
- Chang, W.-L., Wang, H.-P., Peng, W.-H. and Chiu, W.-C., 2019. All about structure: Adapting structural information across domains for boosting semantic segmentation. In: *The IEEE Conference on Computer Vision and Pattern Recognition (CVPR)*. [3](#)
- Chen, D., He, M., Fan, Q., Liao, J., Zhang, L., Hou, D., Yuan, L. and Hua, G., 2019. Gated context aggregation network for image dehazing and deraining. In: *2019 IEEE Winter Conference on Applications of Computer Vision (WACV)*, IEEE, pp. 1375–1383. [1](#), [3](#), [9](#)
- Chen, L.-C., Papandreou, G., Kokkinos, I., Murphy, K. and Yuille, A. L., 2018a. Deeplab: Semantic image segmentation with deep convolutional nets, atrous convolution, and fully connected crfs. *IEEE transactions on pattern analysis and machine intelligence* 40(4), pp. 834–848. [1](#)
- Chen, T., Li, M., Li, Y., Lin, M., Wang, N., Wang, M., Xiao, T., Xu, B., Zhang, C. and Zhang, Z., 2015. Mxnet: A flexible and efficient machine learning library for heterogeneous distributed systems. *arXiv preprint arXiv:1512.01274*. [7](#)
- Chen, Y.-H., Chen, W.-Y., Chen, Y.-T., Tsai, B.-C., Wang, Y.-C. F. and Sun, M., 2017. No more discrimination: Cross city adaptation of road scene segmenters. In: *Computer Vision (ICCV), 2017 IEEE International Conference on*, IEEE, pp. 2011–2020. [1](#), [3](#)
- Chen, Y., Li, W. and Van Gool, L., 2018b. Road: Reality oriented adaptation for semantic segmentation of urban scenes. In: *The IEEE Conference on Computer Vision and Pattern Recognition (CVPR)*. [3](#)
- Cordts, M., Omran, M., Ramos, S., Rehfeld, T., Enzweiler, M., Benenson, R., Franke, U., Roth, S. and Schiele, B., 2016. The cityscapes dataset for semantic urban scene understanding. In: *Proc. of the IEEE Conference on Computer Vision and Pattern Recognition (CVPR)*. [1](#), [6](#), [7](#)
- Dai, D., Sakaridis, C., Hecker, S. and Van Gool, L., 2019. Curriculum model adaptation with synthetic and real data for semantic foggy scene understanding. *International Journal of Computer Vision* pp. 1–23. [1](#), [2](#), [4](#), [6](#), [7](#), [8](#), [9](#)
- Du, Y. and Li, X., 2018. Recursive deep residual learning for single image dehazing. In: *Proceedings of the IEEE Conference on Computer Vision and Pattern Recognition Workshops*, pp. 730–737. [3](#)
- Geiger, A., Lenz, P. and Urtasun, R., 2012. Are we ready for autonomous driving? the kitti vision benchmark suite. In: *2012 IEEE Conference on Computer Vision and Pattern Recognition*, IEEE, pp. 3354–3361. [1](#)
- Golts, A., Freedman, D. and Elad, M., 2019. Unsupervised single image dehazing using dark channel prior loss. *IEEE Transactions on Image Processing*. [3](#)
- Gong, R., Li, W., Chen, Y. and Gool, L. V., 2019. Dlow: Domain flow for adaptation and generalization. In: *The IEEE Conference on Computer Vision and Pattern Recognition (CVPR)*. [3](#)
- Hahner, M., Dai, D., Sakaridis, C., Zaech, J.-N. and Van Gool, L., 2019. Semantic understanding of foggy scenes with purely synthetic data. In: *2019 IEEE Intelligent Transportation Systems Conference (ITSC)*, IEEE, pp. 3675–3681. [4](#), [7](#)
- He, K., Sun, J. and Tang, X., 2010. Single image haze removal using dark channel prior. *IEEE transactions on pattern analysis and machine intelligence* 33(12), pp. 2341–2353. [3](#)
- Hoffman, J., Tzeng, E., Park, T., Zhu, J., Isola, P., Saenko, K., Efros, A. A. and Darrell, T., 2018. Cycada: Cycle-consistent adversarial domain adaptation. In: *Proceedings of the 35th International Conference on Machine Learning, ICML 2018, Stockholm, Sweden, July 10–15, 2018*, pp. 1994–2003. [3](#), [6](#), [9](#)
- Iqbal, J. and Ali, M., 2020a. Mlsl: Multi-level self-supervised learning for domain adaptation with spatially independent and semantically consistent labeling. In: *The IEEE Winter Conference on Applications of Computer Vision (WACV)*. [1](#), [2](#), [3](#), [4](#), [7](#), [8](#), [9](#), [10](#)
- Iqbal, J. and Ali, M., 2020b. Weakly-supervised domain adaptation for built-up region segmentation in aerial and satellite imagery. *ISPRS Journal of Photogrammetry and Remote Sensing* 167, pp. 263–275. [3](#)
- Khodabandeh, M., Vahdat, A., Ranjbar, M. and Macready, W. G., 2019. A robust learning approach to domain adaptive object detection. In: *Proceedings of the IEEE International Conference on Computer Vision*, pp. 480–490. [1](#), [3](#)
- Kim, G., Park, J., Ha, S. and Kwon, J., 2019. Bidirectional deep residual learning for haze removal. In: *Proceedings of the IEEE Conference on Computer Vision and Pattern Recognition Workshops*, pp. 46–54. [3](#), [8](#), [9](#)
- Kim, J.-H., Jang, W.-D., Sim, J.-Y. and Kim, C.-S., 2013. Optimized contrast enhancement for real-time image and video dehazing. *Journal of Visual Communication and Image Representation* 24(3), pp. 410–425. [3](#)

- Kim, J.-H., Sim, J.-Y. and Kim, C.-S., 2011. Single image dehazing based on contrast enhancement. In: 2011 IEEE International Conference on Acoustics, Speech and Signal Processing (ICASSP), IEEE, pp. 1273–1276. [3](#)
- Kim, M. and Byun, H., 2020. Learning texture invariant representation for domain adaptation of semantic segmentation. In: Proceedings of the IEEE/CVF Conference on Computer Vision and Pattern Recognition, pp. 12975–12984. [3](#)
- Lian, Q., Lv, F., Duan, L. and Gong, B., 2019. Constructing self-motivated pyramid curriculums for cross-domain semantic segmentation: A non-adversarial approach. In: The IEEE International Conference on Computer Vision (ICCV). [1, 3, 7, 8](#)
- Liu, W., Yao, R. and Qiu, G., 2019. A physics based generative adversarial network for single image defogging. Image and Vision Computing 92, pp. 103815. [3](#)
- Luo, Y., Zheng, L., Guan, T., Yu, J. and Yang, Y., 2019. Taking a closer look at domain shift: Category-level adversaries for semantics consistent domain adaptation. In: The IEEE Conference on Computer Vision and Pattern Recognition (CVPR). [8](#)
- Mancini, M., Porzi, L., Rota Bulò, S., Caputo, B. and Ricci, E., 2018. Boosting domain adaptation by discovering latent domains. In: The IEEE Conference on Computer Vision and Pattern Recognition (CVPR). [3](#)
- Marsde, M., McGuinness, K., Little, S., Keogh, C. E. and O'Connor, N. E., 2018. People, penguins and petri dishes: adapting object counting models to new visual domains and object types without forgetting. [1](#)
- Morales, P., Klinghoffer, T. and Jae Lee, S., 2019. Feature forwarding for efficient single image dehazing. In: Proceedings of the IEEE Conference on Computer Vision and Pattern Recognition Workshops, pp. 0–0. [3](#)
- Narasimhan, S. G. and Nayar, S. K., 2003. Contrast restoration of weather degraded images. IEEE transactions on pattern analysis and machine intelligence 25(6), pp. 713–724. [1](#)
- Pei, Y., Huang, Y., Zou, Q., Lu, Y. and Wang, S., 2018. Does haze removal help cnn-based image classification? In: Proceedings of the European Conference on Computer Vision (ECCV), pp. 682–697. [3](#)
- Richter, S. R., Vineet, V., Roth, S. and Koltun, V., 2016. Playing for data: Ground truth from computer games. In: B. Leibe, J. Matas, N. Sebe and M. Welling (eds), European Conference on Computer Vision (ECCV), LNCS, Vol. 9906, Springer International Publishing, pp. 102–118. [6](#)
- Ros, G., Sellart, L., Materzynska, J., Vazquez, D. and Lopez, A. M., 2016. The synthia dataset: A large collection of synthetic images for semantic segmentation of urban scenes. In: The IEEE Conference on Computer Vision and Pattern Recognition (CVPR). [1, 6](#)
- Russakovsky, O., Deng, J., Su, H., Krause, J., Satheesh, S., Ma, S., Huang, Z., Karpathy, A., Khosla, A., Bernstein, M. et al., 2015. Imagenet large scale visual recognition challenge. International journal of computer vision 115(3), pp. 211–252. [6](#)
- Sakaridis, C., Dai, D. and Van Gool, L., 2018a. Semantic foggy scene understanding with synthetic data. International Journal of Computer Vision 126(9), pp. 973–992. [1, 2, 3, 4, 6, 7](#)
- Sakaridis, C., Dai, D., Hecker, S. and Van Gool, L., 2018b. Model adaptation with synthetic and real data for semantic dense foggy scene understanding. In: Proceedings of the European Conference on Computer Vision (ECCV), pp. 687–704. [1, 2, 4, 6, 7, 8](#)
- Sankaranarayanan, S., Balaji, Y., Jain, A., Lim, S. N. and Chellappa, R., 2018. Learning from synthetic data: Addressing domain shift for semantic segmentation. In: Proceedings of the IEEE Conference on Computer Vision and Pattern Recognition (CVPR). [3](#)
- Shannon, C. E., 1948. A mathematical theory of communication. Bell system technical journal 27(3), pp. 379–423. [5](#)
- Subhani, M. N. and Ali, M., 2020. Learning from scale-invariant examples for domain adaptation in semantic segmentation. In: Proceedings of the European Conference on Computer Vision (ECCV), pp. 1–17. [1, 2, 3, 7, 8](#)
- Tan, R. T., 2008. Visibility in bad weather from a single image. In: 2008 IEEE Conference on Computer Vision and Pattern Recognition, IEEE, pp. 1–8. [1](#)
- Tsai, Y.-H., Hung, W.-C., Schuster, S., Sohn, K., Yang, M.-H. and Chandraker, M., 2018. Learning to adapt structured output space for semantic segmentation. In: The IEEE Conference on Computer Vision and Pattern Recognition (CVPR). [1, 2, 3, 7, 8, 9](#)
- Vachmanus, S., Ravankar, A. A., Emaru, T. and Kobayashi, Y., 2020. Semantic segmentation for road surface detection in snowy environment. In: 2020 59th Annual Conference of the Society of Instrument and Control Engineers of Japan (SICE), IEEE, pp. 1381–1386. [1](#)
- Vu, T.-H., Jain, H., Bucher, M., Cord, M. and Pérez, P., 2019a. Advent: Adversarial entropy minimization for domain adaptation in semantic segmentation. In: Proceedings of the IEEE Conference on Computer Vision and Pattern Recognition, pp. 2517–2526. [1, 2, 3, 6](#)
- Vu, T.-H., Jain, H., Bucher, M., Cord, M. and Perez, P., 2019b. Dada: Depth-aware domain adaptation in semantic segmentation. In: The IEEE International Conference on Computer Vision (ICCV). [3](#)
- Wu, Z., Shen, C. and Van Den Hengel, A., 2019. Wider or deeper: Revisiting the resnet model for visual recognition. Pattern Recognition 90, pp. 119–133. [4, 6, 7, 8, 9, 10](#)
- Zhang, Y., David, P. and Gong, B., 2017. Curriculum domain adaptation for semantic segmentation of urban scenes. In: The IEEE International Conference on Computer Vision (ICCV). [1](#)
- Zhang, Y., David, P., Foroosh, H. and Gong, B., 2019. A curriculum domain adaptation approach to the semantic segmentation of urban scenes. IEEE transactions on pattern analysis and machine intelligence. [3](#)
- Zhang, Y., Qiu, Z., Yao, T., Liu, D. and Mei, T., 2018a. Fully convolutional adaptation networks for semantic segmentation. In: Proceedings of the IEEE Conference on Computer Vision and Pattern Recognition, pp. 6810–6818. [3](#)
- Zhang, Y., Qiu, Z., Yao, T., Liu, D. and Mei, T., 2018b. Fully convolutional adaptation networks for semantic segmentation. In: Proceedings of the IEEE Conference on Computer Vision and Pattern Recognition, pp. 6810–6818. [3](#)
- Zhao, H., Shi, J., Qi, X., Wang, X. and Jia, J., 2017. Pyramid scene parsing network. In: IEEE Conf. on Computer Vision and Pattern Recognition (CVPR), pp. 2881–2890. [1](#)
- Zou, Y., Yu, Z., Liu, X., Kumar, B. and Wang, J., 2019. Confidence regularized self-training. In: Proceedings of the IEEE International Conference on Computer Vision, pp. 5982–5991. [3, 5](#)
- Zou, Y., Yu, Z., Vijaya Kumar, B. and Wang, J., 2018. Unsupervised domain adaptation for semantic segmentation via class-balanced self-training. In: Proceedings of the European Conference on Computer Vision (ECCV), pp. 289–305. [1, 2, 3, 4, 6, 7, 8, 9, 10](#)